Check for updates

GEOCHEMISTRY

Enceladus-like geochemistry fuels methanogenesis under extreme CO_2 limitation

Vanessa Helmbrecht[1], Frank Postberg[2], Nozair Khawaja[2,3], Robert Reichelt[4], Frieder Klein[5], Dina Grohmann[4], William D. Orsi[1,6]*

Copyright © 2026 The Authors, some rights reserved; exclusive licensee American Association for the Advancement of Science. No claim to original U.S. Government Works. Distributed under a Creative Commons Attribution NonCommercial License 4.0 (CC BY-NC).

Saturn's icy moon Enceladus features chemical signatures consistent with an alkaline soda ocean with H_2 production via hydrothermal water-rock reactions. Chemolithoautotrophic methanogenesis is thermodynamically favorable under these conditions, but it is unknown whether CO_2 scarcity in the alkaline Enceladus soda ocean limits autotrophy. Here, we show that simulated Enceladus' ocean chemistry containing high concentrations of dissolved inorganic carbon and H_2 from mineral-water reactions enables growth of the chemolithoautotroph H_2-oxidizing methanogen *Methanothermococcus okinawensis* until pH 11, far exceeding its previously known pH limit. Transcriptomics revealed that growing cells overcome CO_2 scarcity in the simulated Enceladus soda ocean by overexpressing the reductive acetyl-CoA pathway for CO_2 fixation, which enabled efficient scavenging of CO_2 at extremely low concentrations. The carbon and energy metabolism of *M. okinawensis* was entirely fueled by the abiotic H_2 derived from the simulated Enceladus mineral-water reactions.

INTRODUCTION

Enceladus, a moon of Saturn, is covered in an ice shell with a liquid subsurface ocean beneath (*1*–*4*). Plumes of ice particles and water vapor erupting from fractures in the South Polar region (*2*, *5*) contain signatures of molecular H_2 (*6*) and CH_4 (*7*). Chemical signatures from the plumes (*2*) indicate that Enceladus has an alkaline soda ocean with high concentrations of dissolved inorganic carbon (DIC) primarily in the form of carbonate (CO_3^{-2}) (*3*, *8*). The pH estimates range from 8 (*9*, *10*) to 11.6 (*11*). The rocky core of Enceladus likely has a composition similar to carbonaceous chondrites and is rich in primitive Fe-Mg silicates (*12*). Water-rock reactions, such as serpentinization, are predicted to form secondary minerals and abiotic H_2 on Enceladus (*6*, *12*–*15*). Abiotic H_2 from serpentinization (*16*) fuels chemolithoautotrophic life on Earth (*17*), and therefore, serpentinization on Enceladus makes it a promising extraterrestrial environment for potential life in our solar system (*13*, *18*).

Thermodynamic models predict that the concentrations of H_2 on Enceladus are sufficient to fuel hydrogenotrophic methanogenesis as an energetically favorable metabolism (*6*, *12*, *18*–*20*). Methane (CH_4) was detected in the plumes of Enceladus, but the source of the CH_4 (whether biological or abiotic) remains unknown (*11*, *19*, *21*, *22*). Biological methanogenesis is performed by archaea, which are versatile microorganisms that can tolerate alkaline pH up to 10.2 (*23*, *24*), possibly higher, and temperatures from ~0° to 110°C (*25*, *26*). However, at pH values above 9, chemolithoautotrophic methanogens face an additional challenge: CO_2 scarcity. At pH >9, most of the DIC exists in the form of CO_3^{2-} (and to some extent HCO_3^-). The dominance of CO_3^{2-} in the DIC of Enceladus available to autotrophs may hinder CO_2 fixation due to CO_2 scarcity. Chemolithoautotrophic methanogens depend on CO_2 as a carbon source and are generally optimized to live at circumneutral or slightly acidic pH (*27*). Living at pH <7 is beneficial to cells because most DIC is available as CO_2, which can freely diffuse across the cell membrane (*28*). Laboratory experiments with autotrophic methanogens in Enceladus-like conditions [but at acidic pH ~5; (*29*, *30*)] showed successful CH_4 production. However, it is currently unknown whether chemolithoautotrophic methanogens would be able to grow under the extreme CO_2 scarcity at the alkaline pH of Enceladus' ocean where DIC is dominated by CO_3^{-2}/HCO_3^-.

Here, we experimentally investigated whether cellular growth via chemolithoautotrophic methanogenesis is possible under the high pH of simulated Enceladus ocean-floor conditions. As a model organism, we used the chemolithoautotrophic, thermophilic, H_2-oxidizing methanogen *Methanothermococcus okinawensis* that was isolated from a deep-sea hydrothermal vent (Iheya Ridge, Okinawa Trough, Japan) and was reported to grow at pH up to 8.5 (*31*). *M. okinawensis* belongs to the group of methanogens that lack cytochromes and, as such, has a relatively lower H_2 threshold for growth compared to methanogens that contain cytochromes (*32*). Moreover, methanogens that lack cytochromes usually use sodium gradients for ATP synthesis (*32*). These traits might represent an advantage for *M. okinawensis* in high pH environments, such as the Enceladus soda ocean.

RESULTS AND DISCUSSION

Mineral precipitation in an alkaline Enceladus simulant

We simulated an alkaline Enceladus seafloor environment, here referred to as "Enceladus simulant," which is a mixture of an Enceladus ocean simulant (EOS) and a simulated Enceladus rock powder (SERP) (Fig. 1A and fig. S1). The EOS was prepared over a range of alkaline pH (*10*–*12*) and contained DIC at a concentration of 100 mmol kg^{-1}, which represents the upper end of estimated DIC concentrations (20 to 100 mmol kg^{-1}) in the Enceladus ocean (*3*). This pH range was proposed as thermodynamically favorable for hydrogenotrophic methanogenesis in the Enceladus ocean (*6*, *11*).

[1]Department of Earth and Environmental Sciences, Palaeontology and Geobiology, Ludwig-Maximilians-Universität, 80333 Munich, Germany. [2]Institute of Geological Sciences, Planetary Sciences and Remote Sensing, Freie Universitat Berlin, 12249 Berlin, Germany. [3]German Aerospace Center (DLR e.V.), Institute of Space Research, Rutherfordstraße 2 12489, Berlin, Germany. [4]Institute of Biochemistry, Genetics and Microbiology, Institute of Microbiology and Archaea Centre, Single-Molecule Biochemistry Lab and Regensburg Center for Biochemistry, University of Regensburg, 93053 Regensburg, Germany. [5]Department of Marine Chemistry and Geochemistry, Woods Hole Oceanographic Institution, Woods Hole, MA 02543, USA. [6]GeoBioCenterLMU, Ludwig-Maximilians-Universitat, 80333 Munich, Germany.
*Corresponding author. Email: w.orsi@lrz.uni-muenchen.de

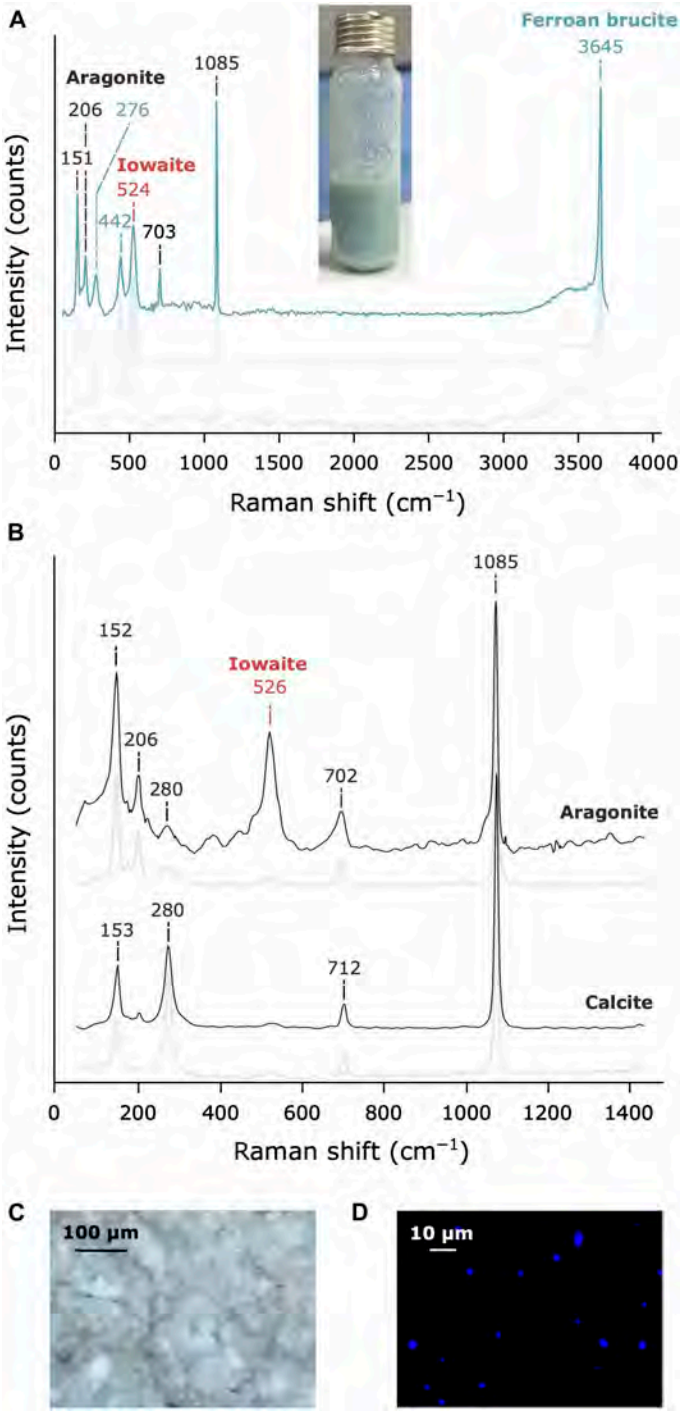


Fig. 1. Mineral precipitates and viable cells in Enceladus simulant experiments. (**A**) Raman spectroscopy of mineral precipitates in the Enceladus simulant after 48 hours. Bands show the presence of ferroan brucite, iowaite, and aragonite. The picture shows the mineral precipitates with a blue-green color. (**B**) Raman spectra from the 0 to 1400 range showing plausible carbonate (aragonite and calcite) and iowaite mineralogy. (**C**) High-magnification photograph of mineral precipitate from the Enceladus simulant. (**D**) Fluorescence microscopy image of intact *M. okinawensis* cells (blue) in the Enceladus simulant after 48 hours; the fluorescence indicates the presence of coenzyme F420 and cellular viability. All results displayed are from pH 9.

The SERP simulated the proposed chondritic composition of the core of Enceladus (*11*, *12*, *33*), containing SiO_2, MgO, FeO, and CaO in powderized form (*34*) (Materials and Methods). This setup is meant to simulate hydrothermal sediments that would accumulate at the base of a hydrothermal vent.

The Enceladus simulants were incubated at 65°C for 48 hours under strictly anoxic conditions (<1 ppm O_2), forming a blue-green precipitate (Fig. 1A). The pH of the Enceladus simulant was measured at the beginning and the end of the experiments, which showed that the pH of the Enceladus simulants did not change more than 0.5 units over the course of the incubation. Raman spectroscopy, scanning electron microscopy, and differential scanning calorimetry–thermogravimetric analysis (DSC-TGA) showed that the precipitate consisted of ferroan brucite ($Mg_xFe^{2+}{}_{1-x}(OH)_2$), iowaite [$Mg_6Fe^{3+}{}_2(OH)_{16}Cl_2$ * $4H_2O$], calcite ($CaCO_3$), and aragonite ($CaCO_3$) (Fig. 1 and fig. S2). Ferroan brucite forms as a secondary mineral in serpentinizing systems (*35*) from the hydration of olivine (Fig. 1A), indicated by Raman bands at 276, 442, and 3645 cm^{-1}. The prominent Raman band at 3645 cm^{-1}, which shifted down from 3650 cm^{-1} for pure magnesian brucite, shows the presence of Fe in brucite (*35*, *36*). DSC-TGA of the Enceladus simulant (fig. S2) revealed two main weight loss events below 200°C and between 345° and 360°C pointing to the dehydroxylation of ferroan brucite (*36*). Energy dispersive x-ray analysis (fig. S2) suggested that the precipitate is chiefly composed of Mg and Fe, namely, 89 mol% Mg and 11 mol% Fe [x in $Mg_xFe^{2+}{}_{1-x}(OH)_2 = 0.097$ to 0.128], which is in the observed range of $x = 0.05$ to 0.35 for ferroan brucite (*37*). Iowaite, a layered double hydroxide (*38*), can form at the expense of ferroan brucite (*35*). Natural iowaite is characterized by a prominent Raman band around 526 cm^{-1} (*38*).

In addition to ferroan brucite and iowaite, calcite and aragonite are present among the mineral precipitates. The Raman band at 1085 cm^{-1} corresponds to calcium carbonates (*39*) while Raman bands at 712 and 702 cm^{-1} are indicative of calcite and aragonite, respectively. Intact *M. okinawensis* cells were observed in Enceladus simulants (Fig. 1D) that were autofluorescent under UV, indicating the presence of coenzyme F420 and cellular viability. Because *M. okinawensis* requires H_2 for growth, we investigated the formation of abiotic H_2 through hydrothermal mineral-water reactions in the Enceladus simulants.

Mineral-water reactions produce abiotic H_2 and fuel chemolithoautotrophic methanogenesis in the Enceladus simulant

In all Enceladus simulants, we detected ample concentrations of abiotic H_2 ranging from 281 ± 5 µM to 166 ± 8 µM (Fig. 2A and table S1). This is well above the minimal levels of H_2 that support growth of cytochrome lacking methanogens, such as *M. okinawensis* (lower limit of 1 to 10 Pa H_2) (*32*). No abiotic H_2 was detectable in controls that did not contain $FeCl_2$, demonstrating that production of abiotic H_2 in the Enceladus simulant was dependent on the presence of $FeCl_2$. This also shows that organic contamination from the reagents or laboratory environment cannot explain the copious amounts of H_2 production observed and that dissolved Fe(II) from the $FeCl_2$ was directly linked to the abiotic H_2 formed over our 48-hour timescale. Our use of 60 mM Fe(II) is higher than predicted Fe(II) concentrations in Enceladus hydrothermal fluids that were found to be in the nanomolar to micromolar range (*34*). Accordingly, the abiotic H_2 formation rates measured in our experiments

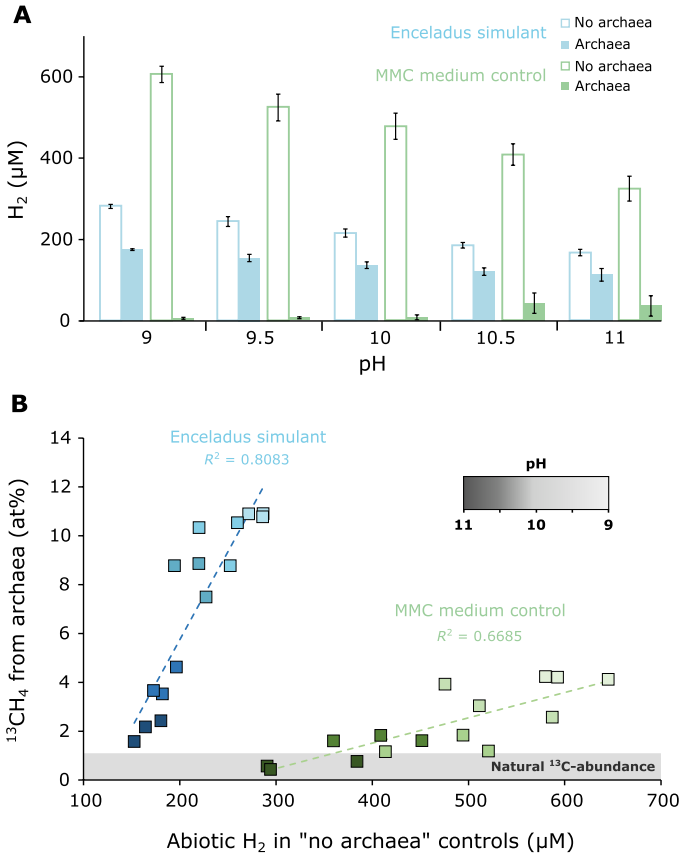


Fig. 2. Mineral-water H_2 production and methanogenesis by *M. okinawensis* in Enceladus simulant compared to controls at pH 9 to 11. (**A**) Concentrations of abiotic H_2 produced via mineral-water reactions in the Enceladus simulant in the absence (unfilled blue bars) and presence (filled blue bars) of *M. okinawensis*. Control experiments with MMC medium (green color) with overpressured headspace H_2/CO_2 gas mixtures are displayed as a comparison. Error bars correspond to standard error of the mean across three biological replicates. (**B**) Stable isotope labeling experiments with $DI^{13}C$ show H_2-dependent $^{13}CH_4$ production in Enceladus simulants (blue) compared to MMC medium controls (green) across the same range of pH (9 to 11) from (A). The highlighted region at the bottom of the plot shows the natural abundance of ^{13}C. ^{13}C-methane at % values above this indicate biological methanogenesis and CO_2 reduction from the added $DI^{13}C$. Total CH_4 production is displayed in fig. S3 confirming a CH_4 increase with decreasing pH.

may exceed those occurring on Enceladus, as our experimental conditions were designed to produce detectable reaction progress on laboratory timescales. The addition of $FeCl_2$ enhanced H_2 production by accelerating thermodynamically favorable reactions between Fe-bearing phases and water that may proceed over geologic timescales. Nevertheless, the measured μM H_2 concentrations in our Enceladus simulants match the predicted H_2 concentration range in Enceladus' soda ocean (*6*), and also fall within the nanomolar to millimolar range predicted for Enceladus hydrothermal fluids (*19*). Similar to previous estimates (*6*, *30*), we measured higher abiotic H_2 formation at relatively lower pH in the Enceladus simulant (Fig. 2A). Abiotic H_2 concentrations in the Enceladus simulants were roughly two to three times lower compared to the MMC medium where H_2 concentrations ranged from 323 ± 30 μM to 605 ± 20 μM.

Ferroan brucite forming in the Enceladus simulant is noteworthy, because it is among the common secondary mineral products of low-temperature serpentinization and linked to H_2 generation (*16*, *35*, *36*, *40*–*42*). Iron in ferroan brucite is in the ferrous state, which is one of the most important factors controlling H_2 concentrations in hydrothermal systems. In hydrothermal and serpentinizing systems, water oxidizes the Fe(II) in ferroan brucite, which increases H_2 flux (*35*, *36*). The dissolution of ferroan brucite results in iowaite formation. Our detection of ferroan brucite, iowaite, and copious amounts of H_2 compared to controls shows that this process was occurring in our setup. When the generated H_2 is consumed, e.g., by microbes, the brucite reaction is pulled forward, generating even more H_2 (*35*). Considering the mineral phases, a possible H_2 generating reaction for Fe-rich brucite to iowaite is shown in Eq. 1

$$8\left(Mg_{0.75}Fe^{2+}_{0.25}\right)(OH)_2 + 6H_2O + 2Cl^- \rightarrow Mg_6Fe^{3+}_2(OH)_{16}Cl_2 * 4H_2O + H_2 + 2OH^- \quad (1)$$

When *M. okinawensis* was added to the Enceladus simulants, the concentrations of H_2 were 38 to 31% lower compared to abiotic controls, indicating that *M. okinawensis* consumed some of the abiotic H_2 (Fig. 2A). Stable isotope labeling experiments (table S1, experiment 3) with ^{13}C-labeled $NaHCO_3$ (Materials and Methods) allowed tracking of ^{13}C-labeled CH_4 produced from the added $DI^{13}C$. Compared to MMC medium, stable isotope labeling experiments showed that *M. okinawensis* exhibited higher rates of methanogenesis correlated to the presence of abiotic H_2 ($R^2 = 0.81$) in the Enceladus simulants at alkaline pH (Fig. 2B). ^{13}C-labeling of CH_4 in the Enceladus simulant varied from 10.9 to 2.1 atomic % (at %) ^{13}C with more $^{13}CH_4$ produced at lower pH. In contrast, *M. okinawensis* produced less $^{13}CH_4$ at alkaline pH in MMC medium, namely, 4.2 to 1.7 at % $^{13}CH_4$ until pH 10.5. At pH 11, no $^{13}CH_4$ production was detectable in the MMC medium (Fig. 2B). In contrast, *M. okinawensis* still produced $^{13}CH_4$ even at pH 11 in the Enceladus simulant to a level of 2.1 at % ^{13}C (Fig. 2B). In addition to the stable isotope labeling, the total amount of methane produced shows the same trends of increased CH_4 production in the Enceladus simulants relative to the MMC medium at alkaline pH, with a positive correlation with H_2 availability (fig. S3).

Despite the MMC medium having higher concentrations of H_2, lower CH_4 production was observed at alkaline pH compared to the Enceladus simulants (fig. S3 and Fig. 2B). This indicates that hydrogenotrophic methanogenesis was limited in the MMC medium at alkaline pH, potentially due to lower CO_2 concentrations. Specifically, at a pH ranging from 9 to 11, the concentration of $CO_{2(aq)}$ in the MMC medium ranges from 10^{-6} to 10^{-10} mol kg^{-1}, whereas in the Enceladus simulants, $CO_{2(aq)}$ was present at concentrations one to two orders of magnitude higher (10^{-5} to 10^{-8} mol kg^{-1}) due to the higher DIC levels.

Abiotic H_2 production fuels autotrophic growth

In line with prior studies (*23*, *31*), *M. okinawensis* grew best at a circumneutral pH of ~6.5 in the MMC medium (table S1) and exhibited an exponential growth phase (growth rate $\mu = 0.12$ $hour^{-1}$) (fig. S4; Materials and Methods) yielding >10^7 cells ml^{-1} after 48 hours. In contrast, in the MMC medium at pH 9, linear growth was observed (Fig. 3A), resulting in 10^5 cells ml^{-1}, a 100-fold reduction compared to growth at pH 6.5 in the MMC medium (fig. S4). At pH 10 in the MMC medium, there was a 10,000-fold reduction in growth compared to pH 6.5. At pH 11, no growth was observed in the MMC medium (Fig. 3, B and C).

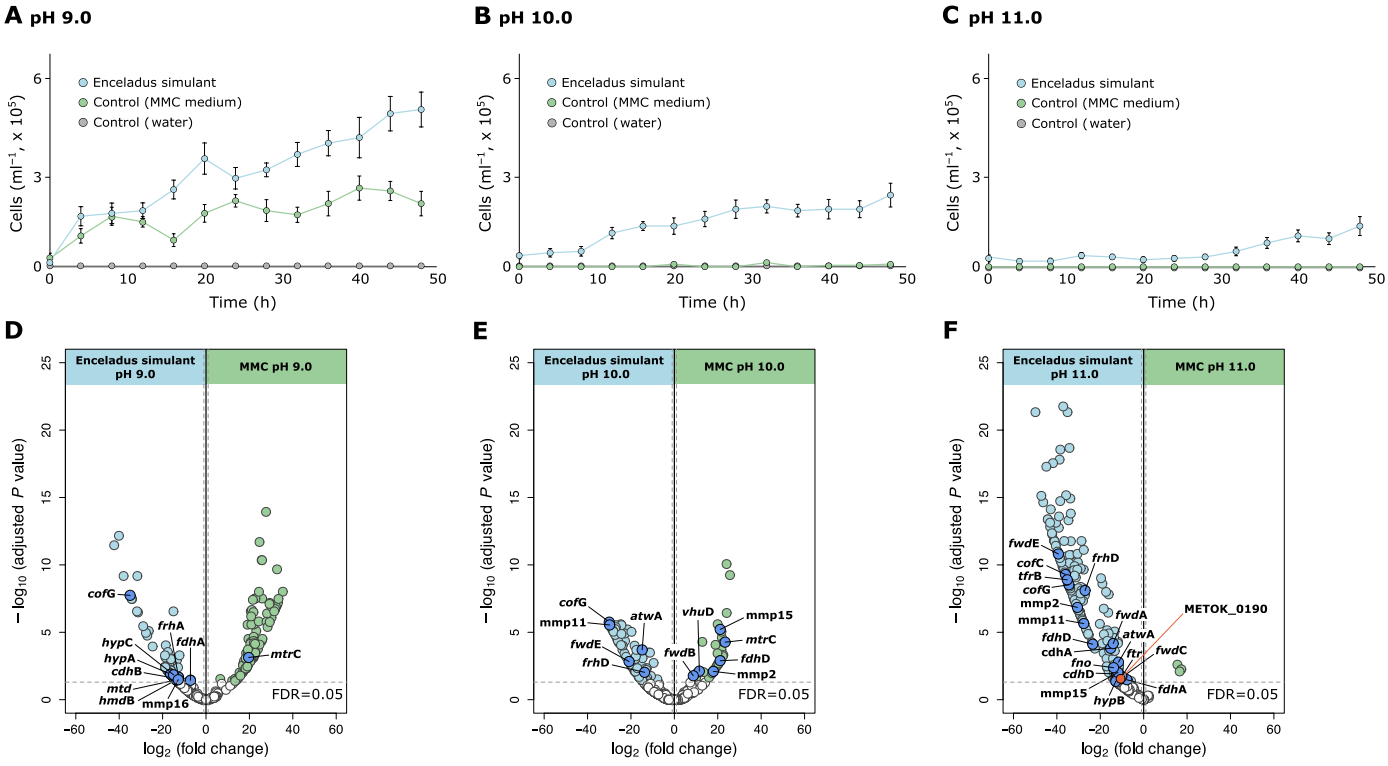


Fig. 3. Increased growth and differential gene expression of *M. okinawensis* in Enceladus simulants compared to MMC medium at pH 9, 10, and 11. (**A** to **C**) Growth curves of *M. okinawensis* at pH 9 (A), pH 10 (B), and pH 11 (C) compared to MMC medium and sterile water controls show an increased growth in the Enceladus simulant at all pH values tested. The highest growth was observed at pH 9 in the Enceladus simulant. Error bars indicate standard error of the mean across three biological replicates (table S1). (**D** to **F**) Volcano plots showing differential gene expression of *M. okinawensis* in the Enceladus simulant compared to MMC medium. Dark blue points highlight genes encoding proteins involved in the reductive acetyl-CoA pathway for methanogenesis as well as H_2 oxidation. The red point in (F) is a gene (Metok_0190) encoding the substrate binding domain of a predicted ABC-type nitrate/bicarbonate transporter. Gene acronyms are listed in table S2.

In the Enceladus simulant, however, *M. okinawensis* showed increased growth compared to the MMC medium at alkaline pH reaching up to 5.3×10^5 cells ml^{-1} after 48 hours at pH 9 (Fig. 3A), 2.5-fold higher compared to MMC medium controls (Fig. 3A). At pH 10 in the Enceladus simulants, cells grew up to slightly lower concentrations compared to pH 9 (2.4×10^5 cells ml^{-1}), but still 100 times higher compared to the MMC controls (Fig. 3B). At pH 11 in the Enceladus simulants, growth was still detectable up to 1.4×10^5 cells ml^{-1} (Fig. 3C) compared to no growth in the MMC medium. To our knowledge, this extends the known pH limit [pH 8.5 (*31*)] of *M. okinawensis* to pH 11. Our findings are consistent with prior studies, showing that autotrophic methanogenesis is possible under alkaline conditions ranging from pH 7 to 12 (*43*–*45*).

Overexpression of reductive acetyl-CoA pathway scavenges CO_2 from Enceladus simulant

Chemolithoautotrophic methanogens, such as *M. okinawensis*, use the reductive acetyl-CoA pathway to fix CO_2 via H_2 reduction, which serves to provide CO_2 as a carbon source for cell growth and produces CH_4 as a metabolic by-product (*46*). We used differential gene expression to investigate the expression of this pathway under the CO_2-limited conditions at alkaline pH in the Enceladus simulant compared to MMC controls. The number of overexpressed genes increased as a function of pH in the Enceladus simulants (fig. S5), whereas in MMC controls, the number of overexpressed genes decreased with increasing pH. A general trend was observed, that under alkaline growth conditions, the number of overexpressed genes increased compared to the growth conditions in MMC at pH 6.5 (fig. S6). At pH 9, 10, and 11, a total of 170, 82, and 255 genes were significantly overexpressed ($P < 0.05$, FDR < 0.05, $|\log_2$ fold change$| \geq 1$) in the Enceladus simulant compared to the MMC medium (Fig. 3, D to F). In MMC medium, 101, 35, and 3 genes were significantly overexpressed relative to the Enceladus simulant at pH 9, 10, and 11, respectively. These results show that a distinct physiological response of *M. okinawensis* was induced by the geochemical conditions of the Enceladus simulant at alkaline pH. This physiological response is mirrored in the overexpression of arCOGs [Archaeal Clusters of Orthologous Genes database (*47*)] in the Enceladus simulant, where energy production and conversion (7 to 11%) was a large portion of the overexpressed genes (33 to 39%) at alkaline pH (fig. S7).

The fixation of CO_2 by *M. okinawensis* at alkaline pH may involve carbonic anhydrase, an enzyme many autotrophic microbes use to convert HCO_3^- to CO_2 (*48*). The genome of *M. okinawensis* encodes several carbonic anhydrases, which were expressed in some alkaline treatments albeit not significantly. However, several genes encoding proteins of the acetyl-CoA pathway for CO_2 fixation were significantly overexpressed at pH 9, 10, and 11 in the Enceladus simulants (Fig. 3, D to F, and table S2). At pH 10, genes encoding proteins of the acetyl-CoA pathway were also overexpressed in the MMC medium control (Fig. 3E).

The highest number of overexpressed genes involved in methanogenesis ($n = 18$ genes) was observed at pH 11 in the Enceladus simulant, relative to the MMC medium control (Fig. 3F). This included overexpression of genes encoding CO dehydrogenase/acetyl CoA synthase subunits (*cdh*A, *cdh*B, and *cdh*D) producing acetyl-CoA for cell growth (*49*). Furthermore, overexpression of genes encoding formylmethanofuran dehydrogenase subunits (*fwd*A, *fwd*C, and *fwd*E) (*50*), formate dehydrogenase subunits (*fdh*A and *fdh*D) (*50*), and methyl-coenzyme M reductase system component A2 (*atw*A) (*51*) was detected (Fig. 3). The marked increase in overexpression of genes encoding proteins of the acetyl-CoA pathway at pH 11 in the Enceladus simulants relative to the MMC controls (Fig. 3F) indicates a role for this metabolism in *M. okinawensis* overcoming CO_2 limitation at pH 11 in the Enceladus simulant. At pH 11, *M. okinawensis* appears to overexpress its CO_2-fixation machinery in response to high DIC concentrations in the Enceladus simulant to scavenge extremely low concentrations of CO_2 for energy conservation and growth.

At high pH, energy limitation due to H^+ scarcity makes it difficult for cells to maintain a proton motive force driving ATP synthesis (*52*). In cytochrome-lacking methanogens such as *M. okinawensis*, however, sodium ion gradients are used for ATP synthesis (*32*), which might help to overcome H^+ scarcity under high pH conditions. Several overexpressed genes were found involving the creation of a Na^+ gradient (Na^+/H^+ antiporters, sodium-extruding oxaloacetate decarboxylase subunit alpha, table S2), and the expression of archaeal ATP synthases was also observed, which can pump both Na^+ and H^+ to generate ATP (*52*). The gene expression data point toward the use of a Na^+ motive force to synthesize ATP as a means to overcome energy limitation and H^+ scarcity at alkaline pH.

High DIC in Enceladus simulants alleviates CO_2 limitation for *M. okinawensis*

Despite the MMC medium containing higher concentrations of H_2, nutrients, and trace metals, *M. okinawensis* growth was limited in the MMC medium at alkaline pH compared to the Enceladus simulants (Fig. 3, A to C). Because the Enceladus simulant has a 10-fold higher DIC concentration compared to the MMC controls, DIC (the carbon source) may be the limiting factor for growth of *M. okinawensis* in MMC controls. In the Enceladus simulant, $CO_{2(aq)}$ ranges from 7.5×10^{-5} to 3.6×10^{-8} mol kg^{-1}, compared to orders of magnitude lower $CO_{2(aq)}$ concentrations in the MMC medium (4.7×10^{-6} to 8.4×10^{-10} mol kg^{-1}) at pH from 9 to 11. The orders of magnitude higher $CO_{2(aq)}$ concentrations in the Enceladus simulants corresponded to higher observed numbers of new cells that formed in the Enceladus simulant compared to the MMC medium (Fig. 4). In the Enceladus simulants at pH 10 and 11, one to two orders of magnitude more cells were observed compared to MMC controls (Fig. 4).

Although the concentration of $CO_{2(aq)}$ is orders of magnitude higher in the Enceladus simulants compared to the MMC medium at pH >9, alkaline conditions cause the majority of DIC to be in the form of either HCO_3^- and CO_3^{-2}. The high pH causes extreme CO_2 limitation for *M. okinawensis*, which requires CO_2 for biomass production, because they cannot directly access HCO_3^- and CO_3^{-2} for carbon fixation. Enzymatic conversion of HCO_3^- to CO_2 via carbonic anhydrase is one mechanism used by autotrophs that live at neutral or alkaline pH to access CO_2. *M. okinawensis* encodes several carbonic anhydrases, which were expressed at pH 11 in the Enceladus simulants, albeit not significantly overexpressed relative to MMC controls.

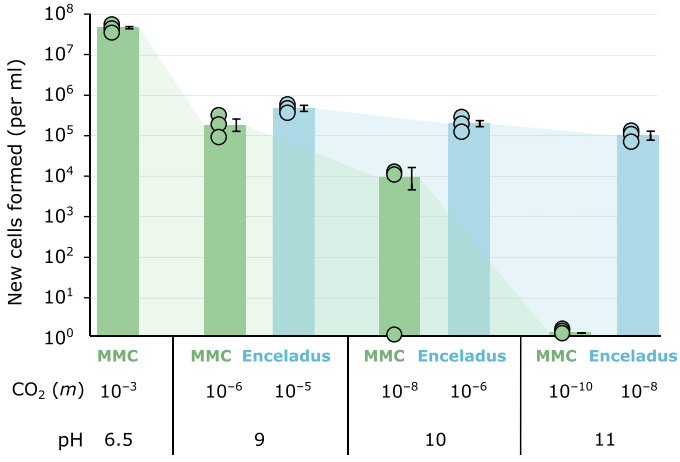


Fig. 4. Increased CO_2 supply in Enceladus simulants promotes chemolithoautotrophic growth of *M. okinawensis* at pH > 9. The number of new cells forming at various pH levels was dependent on the aqueous CO_2 concentrations (molality) in the Enceladus simulant and MMC medium (calculated with SpecE8 in Geochemist's Workbench). The order of magnitude of CO_2 concentration at each pH is displayed underneath each treatment. Note that the CO_2 concentration generally decreases with increasing pH and that the CO_2 concentration in the Enceladus simulant is one to two orders of magnitude higher compared to MMC medium controls at pH 9 to 11.

However, a gene encoding a substrate binding domain of ABC-type nitrate/bicarbonate transporters was significantly overexpressed in the Enceladus simulants at pH 11 relative to MMC controls (Fig. 3F and table S2) and also in the Enceladus simulants at pH 9 and 11 relative to MMC 6.5 (fig. S6). This gene might have been involved in increased HCO_3^- transport in Enceladus simulants, which could be related to the increased growth in Enceladus simulants relative to MMC controls at pH 11.

An alternative mechanism that does not require carbonic anhydrase could be Le Chatelier's Principle, namely, if a system at equilibrium experiences a change (such as removal of CO_2 from an alkaline solution), the equilibrium will shift in the direction that counteracts that change. If *M. okinawensis* cells continuously consume CO_2, more HCO_3^- will convert to CO_2 from the DIC pool to maintain equilibrium. Therefore, at alkaline pH, *M. okinawensis* could still maintain a constant supply of newly formed CO_2, because removal of CO_2 via autotrophy pulls the overall equilibrium to regenerate more CO_2 from HCO_3^-. It is also possible that H_2CO_3 freely diffuses into the cell and is used by the organism (*53*). The overexpression of genes encoding the acetyl-CoA pathway at pH 11 where growth of *M. okinawensis* still occurred (Fig. 3) indicates that the autotrophic metabolism and CO_2 consumption by *M. okinawensis* maintains a constant replenishing of the CO_2 pool from DIC due to Le Chatelier's Principle.

Growth of methanogenic archaea requires numerous trace metals and nutrients that were not added to the Enceladus simulant. The source of trace metals and nutrients must have then been from the small volume of medium (1 ml) that was transferred together with the methanogens when inoculating the Enceladus simulant experiments. This diluted the concentration of trace nutrients by a factor of 20. Despite this, the methanogens still grew better in the Enceladus simulants in comparison to MMC medium showing that trace nutrients were not limiting the growth of *M. okinawensis* in the Enceladus simulants.

The key factor enabling cellular growth under alkaline conditions in the Enceladus simulants is likely the 10-fold higher concentrations of DIC relative to MMC medium. Despite having higher concentrations of available H_2 in the MMC medium (Fig. 2A), reduced cell growth at alkaline pH was observed (Figs. 3 and 4). This can be explained by carbon-limited conditions in the MMC medium at alkaline pH, whereas in the Enceladus simulants, DIC concentrations are high enough to supply CO_2 at levels enabling one to two orders of magnitude higher biomass production.

In summary, our findings potentially widen the habitability window of Enceladus' subsurface soda ocean by demonstrating that the geochemical environment enables the growth of a chemolithoautotrophic methanogen at alkaline pH 9 to 11, far beyond its natural growth range on Earth, by providing two key substrates: abiotic H_2 and DIC at high concentrations. The ability of *M. okinawensis* to grow via the reductive acetyl-CoA pathway under these extreme conditions is consistent with the presence of methanogens (*40*, *44*, *45*, *54*, *55*) and acetogens (*56*, *57*) in hyperalkaline environments generated by serpentinization, potential terrestrial model systems for Enceladus-like geochemistry.

The high carbon abundance in Enceladus' ocean (*3, 4*) has already been found to be a prerequisite for the observed high phosphate availability (*33*) and thus a high DIC appears to be a positive factor for habitability in more than one sense. This high DIC is a consequence of the high carbonate availability for planetary bodies in the solar system that formed beyond the CO_2 snowline, that is, the distance from the Sun beyond which CO_2 is in a solid (icy) state and is available as a planetary building material. Therefore, our findings enhance the habitability potential of subsurface oceans in the outer solar system in a more general sense.

MATERIALS AND METHODS

The Enceladus simulant is an anoxic Enceladus-like microenvironment in the lab that was created to simulate key features of the seafloor of the icy moon. To perform the laboratory experiments, two key features of Enceladus had to be simulated, the rocky core of the icy moon similar to a chondritic composition (*11*, *12*, *33*, *34*) and the overlying soda ocean (*3*, *11*). Because the experiment targets habitability near seafloor hydrothermal environments, the ice crust above the ocean was not taken into account. At the interface of rocky core and ocean, hydrothermal activity is suspected (*12*, *14*). All experiments were conducted in an anoxic chamber (MBraun) with a N_2 atmosphere and O_2 values below 1 ppm. The Enceladus simulant consisted of a SERP and an Enceladus ocean solution (EOS), both mimicking key features of Enceladus' rocky core and soda ocean (Supplementary Methods). Experiments were conducted at an alkaline pH ranging from 9 to 11 (*58*) and at 65°C over 48 hours. In addition, the thermophilic methanogen *M. okinawensis* (DSM strain designation IH1, German Collection of Microorganisms and Cell Cultures GmbH) was added to the Enceladus simulant to test for habitable conditions. All *M. okinawensis* cultures were prepared at the Institute of Microbiology and German Archaea Centre at the University of Regensburg and grown in MMC medium, a common growth medium for methanogens (*59*, *60*). It was previously used to cultivate methanogenic archaea for an early Earth experiment with an iron-sulfide chemical garden (*61*).

RNA extraction was done with the Direct-zol RNA Microprep kit (ZYMO Research) and the protocol from Grünberger *et al.* (*60*) and Helmbrecht *et al.* (*61*). Transcriptomes were sequenced to a median depth of 71.5 (±7.2) million paired end reads and quality trimmed using Seqtk with the default settings (*62*). Quality trimmed reads were searched for similarity against protein encoding genes in the genome of *M. okinawensis* IH1 (*31*) by searching reads via BLASTx against the predicted proteome as a database. Read mappings to specific genes were analyzed as a matrix of mapped reads per gene per sample as described previously (*61*). Differential expression of protein encoding genes and rRNA from the *M. okinawensis* genome across treatments was plotted and analyzed using DESeq2 (*63*), using raw read counts per sample as input with the default settings, in Rstudio. The *SpecE8* program in the Geochemist's Workbench 2025 software version 18.0 using the thermodynamic database thermo.dat (*64*) was used to calculate the aqueous CO_2 concentrations and calcium carbonate mineral saturation states across a range of pH (9, 9.5, 10, 10.5, and 11).

In this study, five different sets of experiments were performed (table S1). Experiment 1 for mineralogical analyses (Fig. 1 and fig. S2), experiment 2 for abiotic H_2 production in the Enceladus simulant (Fig. 2A), experiment 3 for stable isotope labeling (Fig. 2B and fig. S3), experiment 4 to test for growth of *M. okinawensis* in the Enceladus simulant (Fig. 3, A to C, and 4 and fig. S4) and experiment 5 for gene expression analysis (Fig. 3, D to F; figs. S5 to S7; and table S2). Figure S1 gives an overview of all analytical tools used. More details can be found in the Supplementary Materials.

Supplementary Materials

This PDF file includes:

Supplementary Methods
Figs. S1 to S7
Tables S1 to S3

REFERENCES

1. L. Iess, D. J. Stevenson, M. Parisi, D. Hemingway, R. A. Jacobson, J. I. Lunine, F. Nimmo, J. W. Armstrong, S. W. Asmar, M. Ducci, P. Tortora, The gravity field and interior structure of Enceladus. *Science* **344**, 78–80 (2014).
2. C. C. Porco, P. Helfenstein, P. C. Thomas, A. P. Ingersoll, J. Wisdom, R. West, G. Neukum, T. Denk, R. Wagner, T. Roatsch, S. Kieffer, E. Turtle, A. McEwen, T. V. Johnson, J. Rathbun, J. Veverka, D. Wilson, J. Perry, J. Spitale, A. Brahic, J. A. Burns, A. D. DelGenio, L. Dones, C. D. Murray, S. Squyres, Cassini observes the active south pole of Enceladus. *Science* **311**, 1393–1401 (2006).
3. F. Postberg, S. Kempf, J. Schmidt, N. Brilliantov, A. Beinsen, B. Abel, U. Buck, R. Srama, Sodium salts in E-ring ice grains from an ocean below the surface of Enceladus. *Nature* **459**, 1098–1101 (2009).
4. P. Thomas, R. Tajeddine, M. S. Tiscareno, J. A. Burns, J. Joseph, T. J. Loredo, P. Helfenstein, C. Porco, Enceladus's measured physical libration requires a global subsurface ocean. *Icarus* **264**, 37–47 (2016).
5. C. J. Hansen, L. Esposito, A. I. F. Stewart, J. Colwell, A. Hendrix, W. Pryor, D. Shemansky, R. West, Enceladus' water vapor plume. *Science* **311**, 1422–1425 (2006).
6. J. H. Waite, C. R. Glein, R. S. Perryman, B. D. Teolis, B. A. Magee, G. Miller, J. Grimes, M. E. Perry, K. E. Miller, A. Bouquet, J. I. Lunine, T. Brockwell, S. J. Bolton, Cassini finds molecular hydrogen in the Enceladus plume: Evidence for hydrothermal processes. *Science* **356**, 155–159 (2017).
7. J. H. Waite Jr., M. R. Combi, W. H. Ip, T. E. Cravens, R. L. McNutt Jr., W. Kasprzak, R. Yelle, J. Luhmann, H. Niemann, D. Gell, B. Magee, G. Fletcher, J. Lunine, W. L. Tseng, Cassini ion and neutral mass spectrometer: Enceladus plume composition and structure. *Science* **311**, 1419–1422 (2006).
8. F. Postberg, Z. Zou, Y. Sekine, M. Koga, J. Schmidt, M. Fox-Powell, F. Klenner, J. K. Hillier, N. Khawaja, T. Kadono, M. Çakar, S. Kempf, R. Srama, Cassini CDA observes compositional segregation of Enceladus' ice grains from slow freezing and fragmentation of oceanic spray. *Sci. Adv.* **12,** eaee7256 (2026).
9. L. M. Fifer, D. C. Catling, J. D. Toner, Chemical fractionation modeling of plumes indicates a gas-rich, moderately alkaline Enceladus ocean. *Planet. Sci. J.* **3**, 191 (2022).

10. C. R. Glein, J. H. Waite, The carbonate geochemistry of Enceladus' ocean. *Geophys. Res. Lett.* **47**, e2019GL085885 (2020).
11. C. R. Glein, N. Truong, Phosphates reveal high pH ocean water on Enceladus. *Icarus* **441**, 116717 (2025).
12. Y. Sekine, T. Shibuya, F. Postberg, H. W. Hsu, K. Suzuki, Y. Masaki, T. Kuwatani, M. Mori, P. K. Hong, M. Yoshizaki, S. Tachibana, S. I. Sirono, High-temperature water–rock interactions and hydrothermal environments in the chondrite-like core of Enceladus. *Nat. Commun.* **6**, 8604 (2015).
13. M. L. Cable, C. Porco, C. R. Glein, C. R. German, S. M. MacKenzie, M. Neveu, T. M. Hoehler, A. E. Hofmann, A. R. Hendrix, J. Eigenbrode, F. Postberg, L. J. Spilker, A. McEwen, N. Khawaja, J. Hunter Waite, P. Wurz, J. Helbert, A. Anbar, J. P. de Vera, J. Núñez, The science case for a return to Enceladus. *Planet. Sci. J.* **2**, 132 (2021).
14. H.-W. Hsu, F. Postberg, Y. Sekine, T. Shibuya, S. Kempf, M. Horányi, A. Juhász, N. Altobelli, K. Suzuki, Y. Masaki, T. Kuwatani, S. Tachibana, S. I. Sirono, G. Moragas-Klostermeyer, R. Srama, Ongoing hydrothermal activities within Enceladus. *Nature* **519**, 207–210 (2015).
15. A. K. Ramirez-Cabanas, A. Flandes, P. E. Miron-Enriquez, Exploring the general chemistry of the core and ocean of Enceladus. *Adv. Space Res.* **74**, 480–489 (2024).
16. F. Klein, S. Humphris, W. Bach, Brucite formation and dissolution in oceanic serpentinite. *Geochem. Perspect. Lett.* **16**, 1–5 (2020).
17. W. Martin, J. Baross, D. Kelley, M. J. Russell, Hydrothermal vents and the origin of life. *Nat. Rev. Microbiol.* **6**, 805–814 (2008).
18. C. McKay, A. Davila, C. Glein, K. Hand, A. Stockton, "Enceladus astrobiology, habitability, and the origin of life," in *Enceladus and the Icy Moons of Saturn* (University of Arizona Press, 2018), pp. 437-452.
19. A. Affholder, F. Guyot, B. Sauterey, R. Ferrière, S. Mazevet, Putative methanogenic biosphere in enceladus's deep ocean: Biomass, productivity, and implications for detection. *Planet. Sci. J.* **3**, 270 (2022).
20. P. M. Higgins, C. R. Glein, C. S. Cockell, Instantaneous habitable windows in the parameter space of Enceladus' ocean. *J. Geophys. Res. Planets* **126**, e2021JE006951 (2021).
21. F. Klein, J. D. Tarnas, W. Bach, Abiotic sources of molecular hydrogen on Earth. *Elements* **16**, 19–24 (2020).
22. C. P. McKay, C. C. Porco, T. Altheide, W. L. Davis, T. A. Kral, The possible origin and persistence of life on Enceladus and detection of biomarkers in the plume. *Astrobiology* **8**, 909–919 (2008).
23. M. Jebbar, K. Hickman-Lewis, B. Cavalazzi, R. S. Taubner, S. K. M. R. Rittmann, A. Antunes, Microbial diversity and biosignatures: An icy moons perspective. *Space Sci. Rev.* **216**, 10 (2020).
24. R. M. Wormald, S. P. Rout, W. Mayes, H. Gomes, P. N. Humphreys, Hydrogenotrophic methanogenesis under alkaline conditions. *Front. Microbiol.* **11**, 614227 (2020).
25. P. D. Franzmann, Y. Liu, D. L. Balkwill, H. C. Aldrich, E. Conway de Macario, D. R. Boone, *Methanogenium frigidum* sp. nov., a psychrophilic, H2-using methanogen from Ace Lake, Antarctica. *Int. J. Syst. Evol. Microbiol.* **47**, 1068–1072 (1997).
26. M. Kurr, R. Huber, H. König, H. W. Jannasch, H. Fricke, A. Trincone, J. K. Kristjansson, K. O. Stetter, *Methanopyrus kandleri*, gen. and sp. nov. represents a novel group of hyperthermophilic methanogens, growing at 110 °C. *Arch. Microbiol.* **156**, 239–247 (1991).
27. R.-S. Taubner, C. Schleper, M. G. Firneis, S. K.-M. Rittmann, Assessing the ecophysiology of methanogens in the context of recent astrobiological and planetological studies. *Life* **5**, 1652–1686 (2015).
28. L. Steffens, E. Pettinato, T. M. Steiner, A. Mall, S. König, W. Eisenreich, I. A. Berg, High CO_2 levels drive the TCA cycle backwards towards autotrophy. *Nature* **592**, 784–788 (2021).
29. R.-S. Taubner, L. M. F. Baumann, T. Bauersachs, E. L. Clifford, B. Mähnert, B. Reischl, R. Seifert, J. Peckmann, S. K. M. R. Rittmann, D. Birgel, Membrane lipid composition and amino acid excretion patterns of *Methanothermococcus okinawensis* grown in the presence of inhibitors detected in the Enceladian plume. *Life* **9**, 85 (2019).
30. R.-S. Taubner, P. Pappenreiter, J. Zwicker, D. Smrzka, C. Pruckner, P. Kolar, S. Bernacchi, A. H. Seifert, A. Krajete, W. Bach, J. Peckmann, C. Paulik, M. G. Firneis, C. Schleper, S. K. M. R. Rittmann, Biological methane production under putative Enceladus-like conditions. *Nat. Commun.* **9**, 748 (2018).
31. K. Takai, A. Inoue, K. Horikoshi, *Methanothermococcus okinawensis* sp. nov., a thermophilic, methane-producing archaeon isolated from a Western Pacific deep-sea hydrothermal vent system. *Int. J. Syst. Evol. Microbiol.* **52**, 1089–1095 (2002).
32. R. K. Thauer, A. K. Kaster, H. Seedorf, W. Buckel, R. Hedderich, Methanogenic archaea: Ecologically relevant differences in energy conservation. *Nat. Rev. Microbiol.* **6**, 579–591 (2008).
33. F. Postberg, Y. Sekine, F. Klenner, C. R. Glein, Z. Zou, B. Abel, K. Furuya, J. K. Hillier, N. Khawaja, S. Kempf, L. Noelle, T. Saito, J. Schmidt, T. Shibuya, R. Srama, S. Tan, Detection of phosphates originating from Enceladus's ocean. *Nature* **618**, 489–493 (2023).
34. R. Hamp, K. Olsson-Francis, S. Schwenzer, V. Pearson, An inorganic silicate simulant to represent the interior of Enceladus. *Planet. Space Sci.* **248**, 105934 (2024).
35. A. Templeton, E. Ellison, Formation and loss of metastable brucite: Does Fe (II)-bearing brucite support microbial activity in serpentinizing ecosystems? *Philos. Trans. R. Soc. A* **378**, 20180423 (2020).
36. W. Carlin, B. Malvoisin, B. Lanson, F. Brunet, N. Findling, M. Lanson, V. Magnin, T. Fargetton, L. Jeannin, O. Lhote, Fe^{III}-substituted brucite: Hydrothermal synthesis from $(Mg_{0.8}Fe^{II}_{0.2})$-brucite, crystal chemistry and relevance to the alteration of ultramafic rocks. *Appl. Clay Sci.* **234**, 106845 (2023).
37. S. Zhao, Y. Zhao, Z. Wu, F. Lv, G. Lv, L. Liao, Superhigh and ultrafast removal of congo red and methylene blue in the evolution process of ferroan brucite with multiple mechanism. *J. Environ. Chem. Eng.* **11**, 111114 (2023).
38. R. L. Frost, M. O. Adebajo, K. L. Erickson, Raman spectroscopy of synthetic and natural iowaite. *Spectrochim. Acta A Mol. Biomol. Spectrosc.* **61**, 613–620 (2005).
39. C. G. Kontoyannis, N. V. Vagenas, Calcium carbonate phase analysis using XRD and FT-Raman spectroscopy. *Analyst* **125**, 251–255 (2000).
40. W. J. Brazelton, C. N. Thornton, A. Hyer, K. I. Twing, A. A. Longino, S. Q. Lang, M. D. Lilley, G. L. Früh-Green, M. O. Schrenk, Metagenomic identification of active methanogens and methanotrophs in serpentinite springs of the Voltri Massif, Italy. *PeerJ* **5**, e2945 (2017).
41. N. G. Holm, C. Oze, O. Mousis, J. Waite, A. Guilbert-Lepoutre, Serpentinization and the formation of H_2 and CH_4 on celestial bodies (planets, moons, comets). *Astrobiology* **15**, 587–600 (2015).
42. L. Chimiak, E. Hara, A. Sessions, A. Templeton, Glycine synthesis from nitrate and glyoxylate mediated by ferroan brucite: An integrated pathway for prebiotic amine synthesis. *Proc. Natl. Acad. Sci. U.S.A.* **121**, e2408248121 (2024).
43. G. Callander, J. S. Deutzmann, A. M. Spormann, Alkaline hydrogenotrophic methanogenesis in *Methanococcus vannielii* at low carbon dioxide concentrations. *J. CO_2 Util.* **83**, 102788 (2024).
44. T. A. Caro, S. Kashyap, A. E. Maloney, D. W. Hoyt, M. D. Y. Kubo, T. M. Hoehler, A. S. Templeton, Dissolved inorganic carbon supports robust anabolism and methanogenesis in actively serpentinizing rocks. bioRxiv 672207 [Preprint] (2025). https://biorxiv.org/content/10.1101/2025.08.25.672207v1.
45. N. A. Fiore, A. J. Kohtz, D. N. Miller, S. Antony-Babu, D. Pan, C. Lahey, X. Huang, Y. Lu, N. R. Buan, K. A. Weber, Microbial methane production from calcium carbonate at moderately alkaline pH. *Commun. Earth Environ.* **6**, 85 (2025).
46. G. Fuchs, Alternative pathways of carbon dioxide fixation: Insights into the early evolution of life? *Annu. Rev. Microbiol.* **65**, 631–658 (2011).
47. M. Y. Galperin, R. Vera Alvarez, S. Karamycheva, K. S. Makarova, Y. I. Wolf, D. Landsman, E. V. Koonin, COG database update 2024. *Nucleic Acids Res.* **53**, D356–D363 (2025).
48. M. R. Badger, G. D. Price, CO_2 concentrating mechanisms in cyanobacteria: Molecular components, their diversity and evolution. *J. Exp. Bot.* **54**, 609–622 (2003).
49. S. W. Ragsdale, E. Pierce, Acetogenesis and the Wood–Ljungdahl pathway of CO_2 fixation. *Biochim. Biophys. Acta* **1784**, 1873–1898 (2008).
50. T. Watanabe, O. Pfeil-Gardiner, J. Kahnt, J. Koch, S. Shima, B. J. Murphy, Three-megadalton complex of methanogenic electron-bifurcating and CO_2-fixing enzymes. *Science* **373**, 1151–1156 (2021).
51. C. H. Kuhner, B. D. Lindenbach, R. S. Wolfe, Component A2 of methylcoenzyme M reductase system from *Methanobacterium thermoautotrophicum* delta H: Nucleotide sequence and functional expression by Escherichia coli. *J. Bacteriol.* **175**, 3195–3203 (1993).
52. K. Schlegel, V. Leone, J. D. Faraldo-Gómez, V. Müller, Promiscuous archaeal ATP synthase concurrently coupled to Na+ and H+ translocation. *Proc. Natl. Acad. Sci. U.S.A.* **109**, 947–952 (2012).
53. H. M. Miller, N. Chaudhry, M. E. Conrad, M. Bill, S. H. Kopf, A. S. Templeton, Large carbon isotope variability during methanogenesis under alkaline conditions. *Geochim. Cosmochim. Acta* **237**, 18–31 (2018).
54. W. J. Brazelton, J. M. McGonigle, S. Motamedi, H. L. Pendleton, K. I. Twing, B. C. Miller, W. J. Lowe, A. M. Hoffman, C. A. Prator, G. L. Chadwick, R. E. Anderson, E. Thomas, D. A. Butterfield, K. A. Aquino, G. L. Früh-Green, M. O. Schrenk, S. Q. Lang, Metabolic strategies shared by basement residents of the lost city hydrothermal field. *Appl. Environ. Microbiol.* **88**, e0092922 (2022).
55. E. M. Fones, D. R. Colman, E. A. Kraus, R. Stepanauskas, A. S. Templeton, J. R. Spear, E. S. Boyd, Diversification of methanogens into hyperalkaline serpentinizing environments through adaptations to minimize oxidant limitation. *ISME J.* **15**, 1121–1135 (2021).
56. S. Suzuki, S. Ishii, G. L. Chadwick, Y. Tanaka, A. Kouzuma, K. Watanabe, F. Inagaki, M. Albertsen, P. H. Nielsen, K. H. Nealson, A non-methanogenic archaeon within the order *Methanocellales*. *Nat. Commun.* **15**, 4858 (2024).
57. D. R. Colman, E. A. Kraus, P. H. Thieringer, K. Rempfert, A. S. Templeton, J. R. Spear, E. S. Boyd, Deep-branching acetogens in serpentinized subsurface fluids of Oman. *Proc. Natl. Acad. Sci. U.S.A.* **119**, e2206845119 (2022).
58. C. R. Glein, J. A. Baross, J. H. Waite Jr., The pH of Enceladus' ocean. *Geochim. Cosmochim. Acta* **162**, 202–219 (2015).

59. L. Gambelli, M. N. Isupov, R. Conners, M. McLaren, A. Bellack, V. Gold, R. Rachel, B. Daum, An archaellum filament composed of two alternating subunits. *Nat. Commun.* **13**, 710 (2022).
60. F. Grünberger, G. Schmid, Z. el Ahmad, M. Fenk, K. Vogl, R. Reichelt, W. Hausner, H. Urlaub, C. Lenz, D. Grohmann, Uncovering the temporal dynamics and regulatory networks of thermal stress response in a hyperthermophile using transcriptomics and proteomics. *MBio* **14**, e0217423 (2023).
61. V. Helmbrecht, R. Reichelt, D. Grohmann, W. D. Orsi, Simulated early Earth geochemistry fuels a hydrogen-dependent primordial metabolism. *Nat. Ecol. Evol.* **9**, 769–778 (2025).
62. H. Li, seqtk Toolkit for processing sequences in FASTA/Q formats. *GitHub* **767**, 69 (2012).
63. M. I. Love, W. Huber, S. Anders, Moderated estimation of fold change and dispersion for RNA-seq data with DESeq2. *Genome Biol.* **15**, 550 (2014).
64. C. M. Bethke, *Geochemical and Biogeochemical Reaction Modeling* (Cambridge Univ. Press, 2021).

Acknowledgments: We would like to thank K. Olsson-Francis for discussions and M. Kaliwoda for providing access to the Raman Spectroscope at the Bavarian State Collection for Mineralogy in Munich. **Funding:** This work was supported by the Deutsche Forschungsgemeinschaft project OR 417/8-1 granted to W.D.O. The work was also supported in part by the Transregio Collaborative Research Center (CRC 392, "Molecular Evolution in Prebiotic Environments") granted to W.D.O. N.K. was supported by the European Research Council under the consolidator grant no. 101171589-AIMS. **Author contributions:** Conceptualization: V.H., F.P., N.K., W.D.O., and D.G. Methodology: V.H., R.R., F.P., D.G., and W.D.O. Formal analysis: W.D.O., V.H., F.K., and N.K. Resources: W.D.O., D.G., V.H., R.R., and F.K. Investigation: V.H., W.D.O., and F.K. Validation: W.D.O., V.H., F.K., and F.P. Visualization: V.H., F.K., and W.D.O. Funding acquisition: W.D.O. and D.G. Project administration: W.D.O. and D.G. Supervision: W.D.O., F.P., and N.K. Software: V.H. and W.D.O. Data curation: V.H., N.K., and W.D.O. Writing—original draft: V.H. and W.D.O. Writing—review and editing: V.H., N.K., F.P., R.R., F.K., D.G., and W.D.O. **Competing interests:** The authors declare that they have no competing interests. **Data, code, and materials availability:** All data and code needed to evaluate and reproduce the results in the paper are present in the paper and/or the Supplementary Materials. This study did not generate new materials. Transcriptome data have been deposited in the NCBI short read archive under Bioproject ID: PRJNA1157004 (https://ncbi.nlm.nih.gov/bioproject/?term=PRJNA1157004).

Submitted 14 April 2026
Accepted 13 August 2026
Published 25 September 2026
10.1126/sciadv.aei0167